PIER C

(Received 25 September 2024, Accepted 15 October 2024, Scheduled 28 October 2024)

Small Size Radially Embedded Probe-Fed Dielectric Resonator Antenna for Ultra-Wideband Applications

Abinash Thakur and Satyajib Bhattacharyya*

School of Engineering, Tezpur University, Napaam 784028, India

ABSTRACT: Radially embedded probe-fed circular disc dielectric resonator antenna (DRA) for ultrawideband applications is investigated. Initially, a single-layer probe fed DRA is developed. The probe length is adjusted to optimize S_{11} performance. For a probe length of 10 mm, a measured -10 dB bandwidth of 47.8% (4.75–7.74 GHz) is obtained. The design is modified with two concentric rings of different dielectric materials with a hollow center. The modified configuration improves the matching from an S_{11} value of -18 dB at 5.23 GHz to -24.2 dB at 4.56 GHz. However, the measured -10 dB bandwidth reduces to some extent to 38.4% (4.2–6.2 GHz). In another modified design, an air gap is introduced between two inner discs of Alumina supported by a solid outer ring of Teflon. The radially embedded feeding probe, therefore, protrudes into the circular air pocket sandwiched between the two Alumina discs. An improved measured bandwidth of 55.9% (6.66–11.83 GHz) is obtained. Measured S_{11} of -24.1 dB is similar to that obtained for the concentric ring design but at a higher frequency of 9 GHz. All three antenna designs feature a reduced size with a volume of approximately 1963.5 mm^3, wider bandwidth, and consistent radiation patterns over the operating frequency band. It makes the proposed designs suitable for ultra-wideband (UWB) applications.

1. INTRODUCTION

Federal Communications Commission (FCC) has specified ultra-wideband (UWB) technology and approved the release of an unlicensed spectral frequency band of 3.1–10.6 GHz [1]. This UWB technology possesses characteristics such as high data rate transmission in short range, low power consumption, more precise positioning capabilities, and minimum multipath interference [2], making it suitable for applications that include mobile communication [3], audio streaming, augmented reality, smart home, and monitoring applications for hospitals and military use. Reported UWB radar includes railSAR [4], boomSAR [5], SIRE radar [6], SAFIRE radar [7] to detect landmines, and military targets while [8], [9], [10] are used for human detection and monitoring conditions of patients in hospital. In recent years, major brands such as Apple, Samsung, Google, and Xiaomi launched UWB enabled devices [11]. Impedance matching over the required bandwidth, size minimization, consistent gain, and radiation pattern over the operating band are some of the major design challenges [12–14]. In recent years, numerous types of antennas have been developed for UWB applications. These include Vivaldi antenna for low radar cross section (RCS) applications [15], slot antenna for modern UWB communication systems [16], metal waveguide slot array antenna for harsh environments [17], and resonant cavity antenna [18]. Other reported antennas include printed circuit board integrated planar circular disc monopole antenna [19], compact dielectric resonator antenna (DRA) with band-notched characteristics [20], and DRA having consistent omnidirectional radiation patterns over the bandwidth for indoor communication systems [21]. Although Vivaldi and array antennas are preferred in UWB radars, printed antennas and DRAs are more suitable for small electronic devices in indoor communication and positioning applications. Even though the conventional DRAs exhibit better bandwidth (typically 10%) than other low-profile, small-size antenna such as conventional patch antennas (typically 2–5%) [22], they need special design modifications to achieve UWB performance. Techniques include stacked DRAs with the same or different materials [23], separating the resonator from ground plane with an air gap [24], introducing multisegmented dielectric resonator antennas [25], creating air gap inside the resonator [26] and feeding the DRA by a patch [27].

Antenna size is crucial because of the space limitation in UWB communication devices. The overall size of many antennas becomes large owing to the large ground plane or substrate used in them [28–30]. Efforts of addressing this problem with antenna size is reported in [31] where a square-shaped DRA having no additional ground plane except the flange of the coaxial probe is designed. Another DRA reported in [32] is designed with a ground plane of the same size as that of the resonating element.

This article discusses radially embedded probe-fed circular disc DRAs and explores different geometric configurations to achieve wide bandwidth. The feeding probe is embedded radially as against the conventional approach of probe feeding along the normal of the resonator faces. Three antenna configurations of the same volume (1963.5 mm^3) are discussed, which will be referred to hereon as Ant. I, Ant. II, and Ant. III. In

* Corresponding author: Satyajib Bhattacharyya (satyajib@gmail.com).

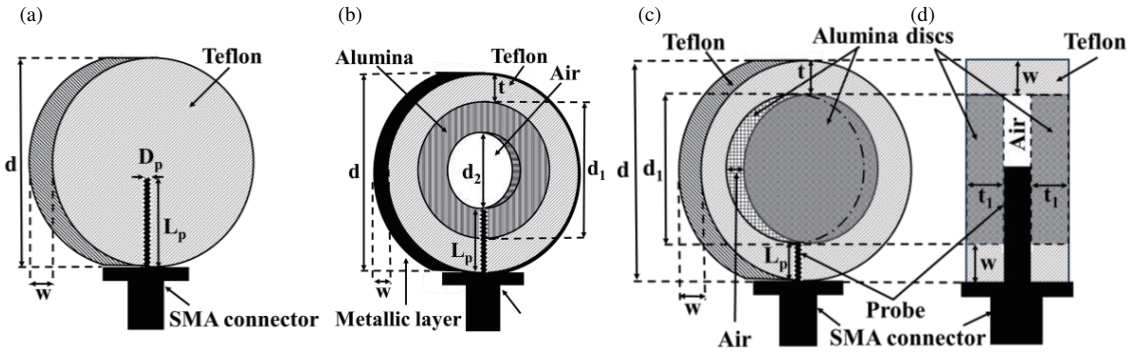

FIGURE 1. Configuration of DRAs: (a) Ant. I (b) Ant. II (c) Ant. III (d) Side view of Ant. III. $d = 25\,\text{mm}$, $w = 4\,\text{mm}$, $d_1 = 15\,\text{mm}$, $d_2 = 8\,\text{mm}$, $t = 5\,\text{mm}$, $t_1 = 1.5\,\text{mm}$, $D_p = 0.9\,\text{mm}$, $L_p = variable$.

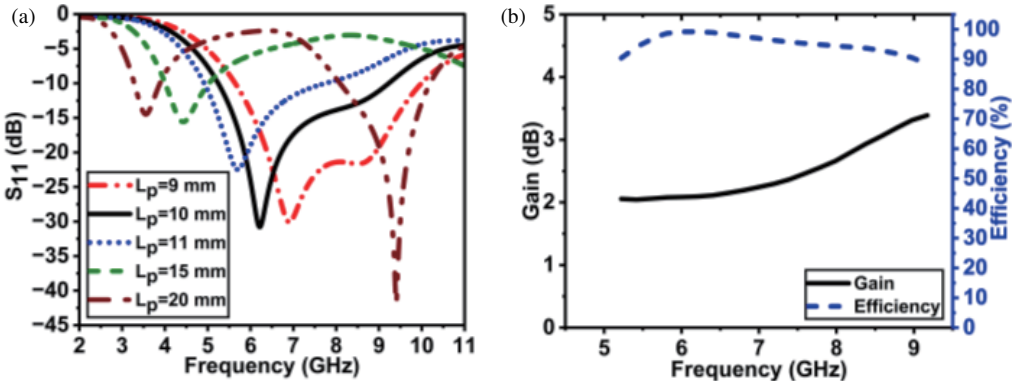

FIGURE 2. (a) Simulated S_{11}-parameters for different probe lengths (L_p) for Ant. I. (b) Simulated gain and efficiency for Ant. I ($L_p = 10\,\text{mm}$).

conventional DRAs, resonators are placed on a metallic ground plane or a dielectric substrate with a metallic layer while the proposed Ant. I and Ant. III have no additional ground plane. For Ant. II, an annular outer metallic ring around the outer cylindrical surface of the resonator is used instead of the conventional planar ground. In general, a resonator mounted on a much larger ground plane leads to a broadside radiation pattern [33, 34]. The approach of eliminating ground plane or using cylindrically conformal ground plane leads to an omnidirectional pattern behavior as well as reduced size.

2. ANTENNA CONFIGURATION AND SIMULATED RESULTS

An initial estimation for the design specifications of the resonator is carried out using [22] and [35]. The estimated dimensions are used to computationally assess antenna performance using CST STUDIO SUITE Learning edition. The design parameters are chosen such that the operating frequency band lies in the UWB allocated frequency band. Different configurations with two dielectric materials are studied. As against the conventional approach of mounting the DRA on a metallic ground plane or a dielectric substrate with a metallic layer, Ant. I [Figure 1(a)] comprises a single homogeneous dielectric (Teflon, $\varepsilon_r = 2.1$) disc excited by a radially inserted probe of diameter (D_p) 0.9 mm which is an extension of the center conductor of the SubMiniature version A (SMA) connector with its flange serving as the ground plane. The simulated S_{11}-parameters for different probe lengths are shown in Figure 2(a). Simulated bandwidths of 55.6% (5.64–9.98 GHz), 55% (5.24–9.22 GHz), 44.7% (4.91–7.74 GHz), 22.6% (4–5.02 GHz), and 16.7% (3.28–3.88 GHz) are observed for probe lengths (L_p) of 9 mm, 10 mm, 11 mm, 15 mm, and 20 mm, respectively.

Ant II [Figure 1(b)] comprises two concentric rings, the outer one of Teflon ($\varepsilon_r = 2.1$) having an inner diameter (d_1) of 15 mm with a thickness (t) of 5 mm and the inner one of Alumina ($\varepsilon_r = 9.8$) with an inner diameter (d_2) of 8 mm and thickness of 3.5 mm. Since high permittivity material leads to lowering bandwidth, and low permittivity material leads to poor coupling between probe and resonator, Alumina is chosen as the best choice due to its medium range of permittivity. Other design parameters such as inner diameter of the outer ring are estimated from computational results. The configuration has an air pocket of a diameter (d_2) of 8 mm at the center. A metallic layer of thickness 0.05 mm is attached to the cylindrical outer surface of the structure. For different probe lengths, S_{11}-parameter results [Figure 3(a)] are observed. A bandwidth of 50.8% (3.34–5.62 GHz) is observed for a probe length (L_p) of 8.5 mm.

Ant. III [Figure 1(c)] consists of a dielectric ring (Teflon, $\varepsilon_r = 2.1$) of inner diameter (d_1) 15 mm with a thickness (t) of 5 mm. Two dielectric discs (Alumina, $\varepsilon_r = 9.8$) of diameter (d_1) 15 mm and thickness (t_1) of 1.5 mm are placed on both faces of the open center of the ring as caps resulting in an air pocket of thickness 0.9 mm between the discs. The exci-

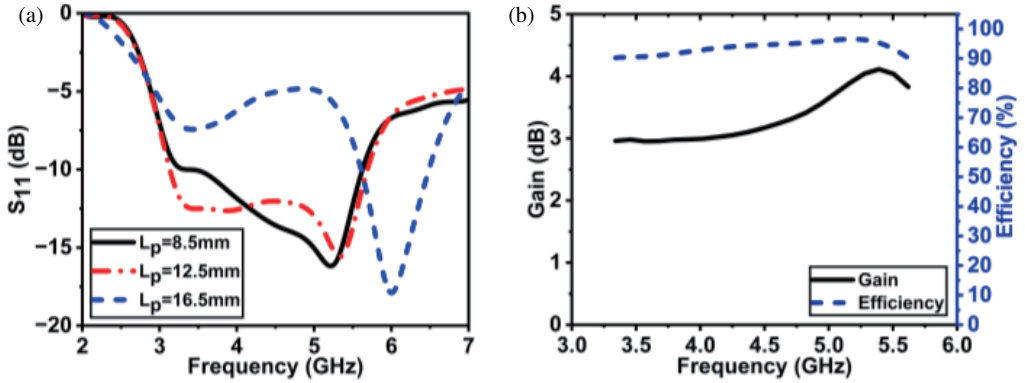

FIGURE 3. (a) Simulated S_{11}-parameters for various probe lengths (L_p) for Ant. II. (b) Simulated gain and efficiency for Ant. II ($L_p = 8.5$ mm).

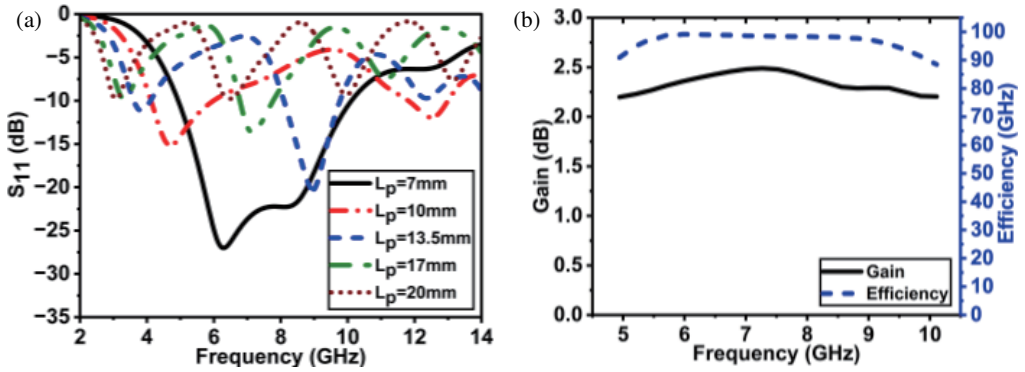

FIGURE 4. (a) Simulated S_{11}-parameters for different probe lengths (L_p) for Ant. III. (b) Simulated gain and efficiency for Ant. III ($L_p = 7$ mm).

tation probe which is an extension of the center conductor of the SMA connector is inserted radially and symmetrically through the dielectric ring and positioned between the dielectric discs at the center with an air gap of 0.9 mm between them. Figure 4(a) shows simulated S_{11}-parameters for probe lengths (L_p) of 7 mm, 10 mm, 13.5 mm, 17 mm, and 20 mm. A 10-dB bandwidth of up to 68.7% (4.94–10.11) is observed.

Simulated gains and efficiency over the operating band for Ant. I, Ant. II, and Ant. III are shown in Figure 2(b), Figure 3(b), and Figure 4(b), respectively. Computational result show antenna efficiencies in excess of 88% for all three configurations. Figure 5 shows the E- and H-fields at the resonating frequency for the respective antennas. It is observed that the E-field is the strongest along the probe while the H-field is circular around the probe. The field distribution is indicative of a transverse magnetic mode.

3. EXPERIMENTAL RESULTS AND DISCUSSION

Measured permittivity, permeability, and loss tangent of Teflon used to fabricate the antennas are reported in [36] as shown in Figure 6(a). Experimental characterizations are carried out using Agilent E8362C PNA Series Vector Network Analyzer. S_{11}-parameters are measured for Ant. I [Figure 1(a)] with probe lengths of 9 mm, 10 mm, 11 mm, 15 mm, and 20 mm [Figure 6(b)]. It is observed that a maximum bandwidth of 47.8% (4.75–7.74 GHz) is obtained for a probe length of 10 mm. The bandwidth and resonant frequency are inversely related to the probe length [Figure 7].

For Ant. II [Figure 1(b)], S_{11}-parameters are measured for probe lengths of 8.5 mm, 12.5 mm, and 16.5 mm while maximum bandwidth is obtained for a probe length of 8.5 mm [Figure 8(a)]. Matching is improved from an S_{11} value of -18 dB for Ant. I to -24.2 dB for Ant. II at the resonant frequency, while the resonant frequency shifts from 5.23 GHz to 4.56 GHz, resulting in size reduction. A measured impedance of $35.5 + j1.1$ and $50.3 - j7.1$ is found for Ant. I and Ant. II at 5.49 GHz and 4.67 GHz, respectively [Figure 8(b)]. However, in the case of Ant. II, the measured -10 dB bandwidth decreases somewhat to 38.4% (4.2–6.2 GHz).

S_{11} parameters are measured for Ant. III [Figure 1(c)] with probe lengths of 7 mm, 10 mm, 13.5 mm, 17 mm, and 20 mm [Figure 9(a)] using Anritsu MS46322B Vector Network Analyzer. A maximum -10 dB bandwidth of 55.9% (6.66–11.83 GHz) is obtained for a probe length of 7 mm. The improvement of bandwidth is observed compared to Ant. I and Ant. II. Improved matching observed in Ant. II is also maintained in Ant. III with an S_{11} value of -24.1 dB while the resonant frequency shifts to 9 GHz, affecting the antenna size. Figure 9(b) shows the fabricated prototypes of all three antenna configurations. A comparative study between the proposed designs and their respective advantages in terms of their bandwidth, size, and design simplicity are highlighted in Table 1.

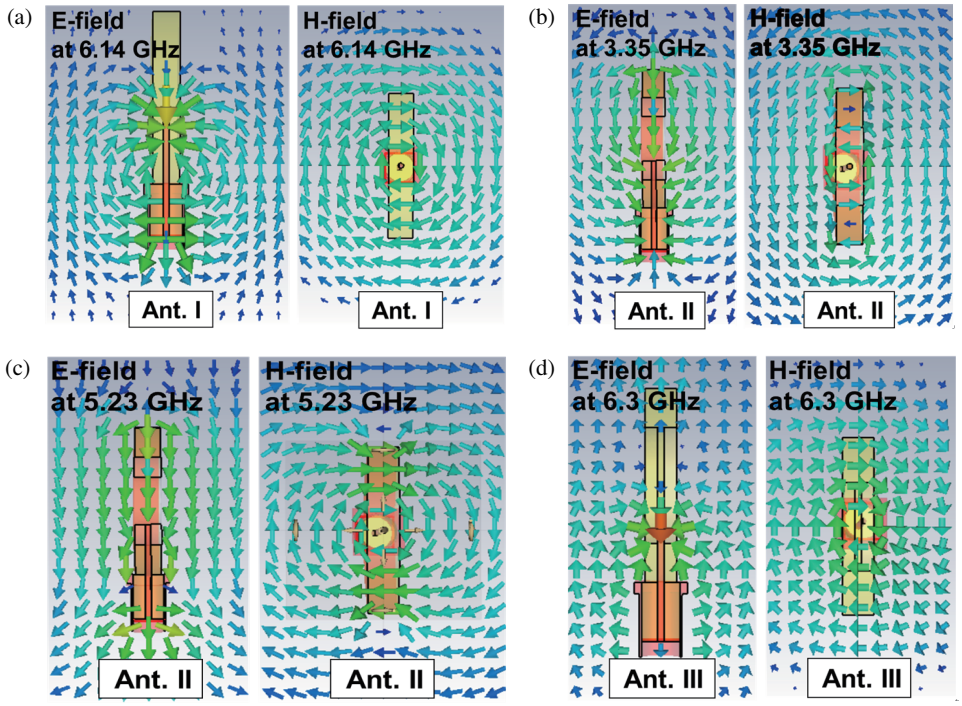

FIGURE 5. (a) Ant. I: E- & H-field (6.14 GHz). (b) Ant. II: E- & H-field (3.35 GHz). (c) Ant. II: E- & H-field (5.23 GHz). (d) Ant. III: E- & H-field (6.3 GHz).

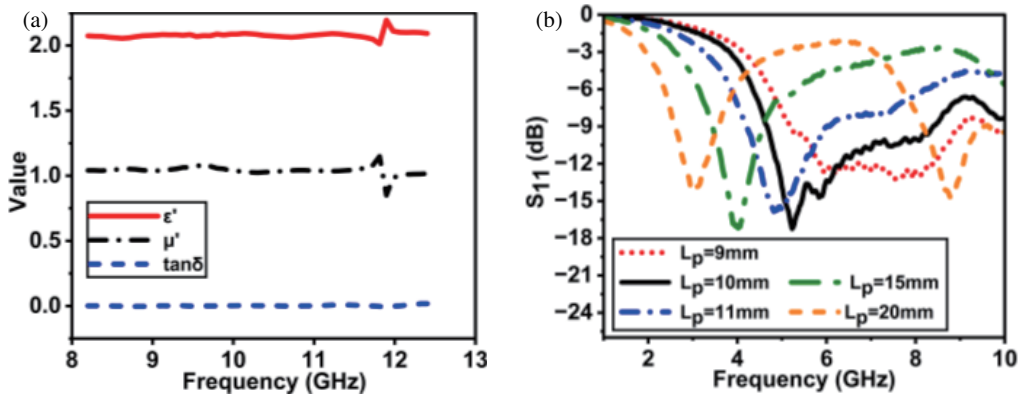

FIGURE 6. (a) Measured permittivity (ε'), permeability (ε'') and loss tangent ($\tan\delta$) [19]. (b) Measured S_{11} results for Ant. I.

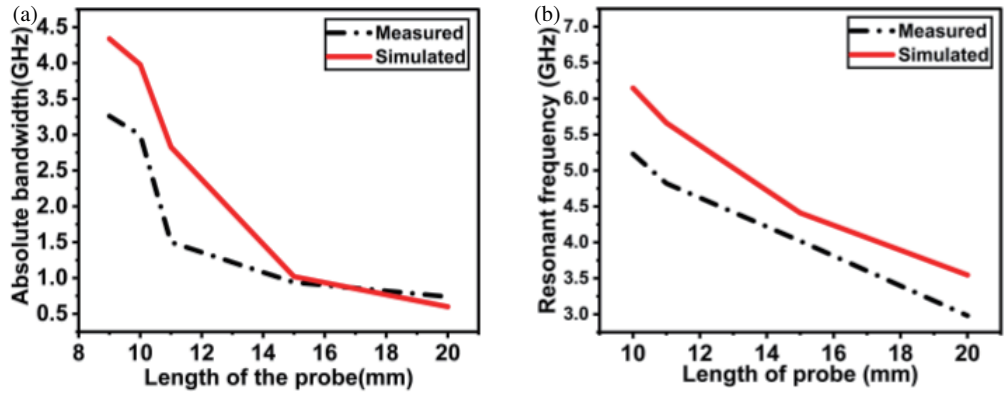

FIGURE 7. (a) Absolute bandwidth versus probe length. (b) Resonant frequency versus probe length.

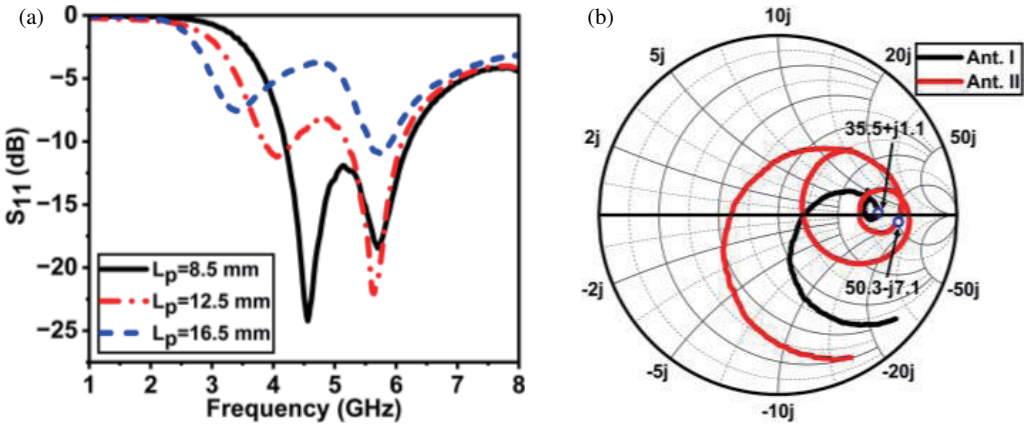

FIGURE 8. (a) Measured S_{11} results for Ant. II. (b) Measured Smith chart for Ant. I and Ant. II.

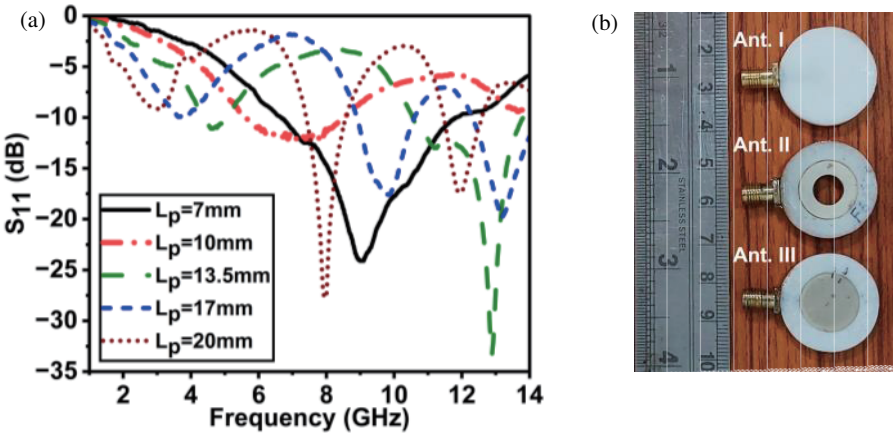

FIGURE 9. (a) Measured S_{11} results for Ant. III. (b) Photograph of the fabricated prototypes.

TABLE 1. Comparison of antenna performance showing best bandwidth for Ant. III.

Parameter	Comparison	Comments
Bandwidth	Ant. II $<$ Ant. I $<$ Ant. III	Ant. III achieves maximum bandwidth.
Size	Ant. II $<$ Ant. I $<$ Ant. III	Normalized antenna size is smaller for Ant. II.
Design simplicity	Ant. III $<$ Ant. II $<$ Ant. I	Although all three designs are simple, Ant. I have the simplest geometry.

Radiation pattern measurements are carried out for all three structures: Ant. I, Ant. II, and Ant. III and are shown in Figure 10. The radiation patterns for Ant. I are measured at the resonant frequency of 4.82 GHz. For Ant. II, radiation patterns are measured at the two S_{11} peaks (4.56 GHz and 5.7 GHz) observed. The radiation patterns for Ant. III are measured at three different frequencies of 7 GHz, 9 GHz, and 11 GHz to ascertain the pattern stability over the bandwidth, since a wide bandwidth of 5.17 GHz is observed for this design. Measured results show that the radiation patterns are omnidirectional in general and remain relatively consistent at these frequencies indicating suitability for application in UWB communication devices requiring omnidirectional radiation properties.

Performance comparison of the proposed DRAs with reported results in terms of their bandwidth and size is summarized in Table 2. It may be noted that Ant. I and Ant. III use no additional ground plane except the in-built connector flange, similar to the design approach reported in [31]. The designed

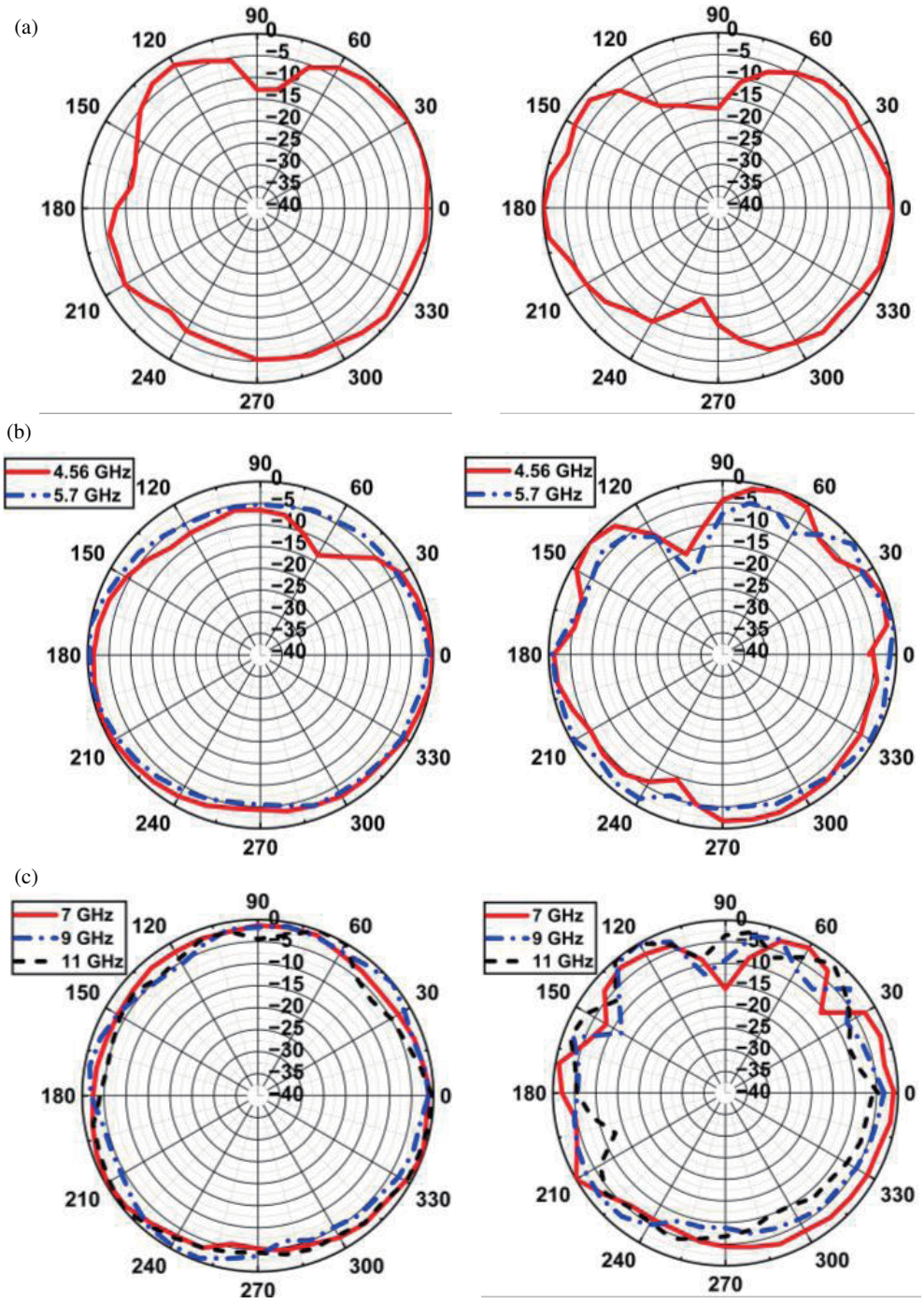

FIGURE 10. Measured radiation patterns for (a) Ant. I, (b) Ant. II and (c) Ant. III. (*Left:* Plane perpendicular to the disc and probe. *Right:* Plane perpendicular to the disc).

antenna structures are seen to be smaller by a factor of as much as 3.5 compared to the structure reported in [31], even while a 12 times larger bandwidth is obtained in the case of Ant. III. Compared with [30], where the use of a ground plane does not increase the antenna profile, Ant. III achieves a 7.6 times larger bandwidth. The DRAs reported in [28], [29], [30], and [37] exhibit a wide bandwidth, but their large ground plane and high profile increase the overall antenna size. Referring to [38] and [39], it is seen that Ant. III achieves a relatively wider bandwidth with a compact size. The wide bandwidth with a compact size and consistent radiation pattern makes the proposed designs suitable for UWB communication devices. Additional uses could be similar to the short-range data transfer application that has been reported in [40], audio streaming, wireless monitor video transmission, smart home gadgets, and military applications [3–10].

TABLE 2. Comparison between current and existing DRAs.

Ref.	Antenna type	ε_r	Size (mm)	Size (λ_0)	Absolute BW [Freq. range] (GHz)	BW (%)
[31]	LP RDRA (No ground plane), 10	10	$31 \times 31 \times 24\,\text{mm}^3$	$0.54 \times 0.54 \times 0.42\lambda_0^3$	0.13 [5.18–5.31]	2.47
	CP RDRA (No ground plane)	10	$31 \times 31 \times 24\,\text{mm}^3$	$0.54 \times 0.54 \times 0.42\lambda_0^3$	0.24 [5.13–5.37]	4.6
[32]	DRA with small ground plane	10	$27 \times 27 \times 14.5\,\text{mm}^3$	$0.22 \times 0.22 \times 0.12\lambda_0^3$	0.18 [2.39–2.57]	7.3
[28]	Stacked triangular prism-shaped DRA	10.2 & 4.4	$140 \times 140 \times 18.9\,\text{mm}^3$	$3.9 \times 3.9 \times 0.53\lambda_0^3$	10.1 [3.3–13.4]	120.9
[29]	Compact stacked cylinder DRA	10.2	$50 \times 50 \times 7.5\,\text{mm}^3$	$1.58 \times 1.58 \times 0.24\lambda_0^3$	7.5 [5.7–13.2]	79.3
[30]	3D printed DRA,	10 & 3	$60 \times 55 \times 23\,\text{mm}^3$	$1.47 \times 1.35 \times 0.57\lambda_0^3$	5.14 [4.8–9.94]	69.7
[37]	Multi-layer DRA	10.2	$30 \times 30 \times 5.08\,\text{mm}^3$	$0.81 \times 0.81 \times 0.14\lambda_0^3$	6.51 [4.8–11.31]	92
[38]	Low profile DRA	15	$132 \times 132 \times 15\,\text{mm}^3$	$1.02 \times 1.02 \times 0.12\lambda_0^3$	0.96 [1.85–2.81]	41.2
[39]	Embedded stacked DRA	3.45 & 9.9	$60 \times 60 \times 15\,\text{mm}^3$	$1.98 \times 1.98 \times 0.49\lambda_0^3$	2.25 [8.75–11]	22.8
Ant. I	Circular disc DRA	2.1	$d = 25\,\text{mm}$, $w = 4\,\text{mm}$	$d = 0.42\lambda_0$, $w = 0.07\lambda_0$	2.99 [4.75–7.74]	47.8
Ant. II	Circular disc DRA	2.1 & 9.8	$d = 25\,\text{mm}$, $w = 4\,\text{mm}$	$d = 0.43\lambda_0$, $w = 0.06\lambda_0$	2 [4.2–6.2]	38.4
Ant. III	Circular disc DRA	2.1 & 9.8	$d = 25\,\text{mm}$, $w = 4\,\text{mm}$	$d = 0.77\lambda_0$, $w = 0.12\lambda_0$	5.17 [6.66–11.83]	55.9

Ref.: reference, BW: $-10\,\text{dB}$ bandwidth, LP: linearly polarized, RDRA: rectangular dielectric resonator antenna, CP: circularly polarized, λ_0: free space wavelength at center frequency, d: diameter, w: width.

4. CONCLUSION

In this article, radially embedded probe-fed DRAs are investigated with three different geometries with the same overall size: Ant. I, Ant. II, and Ant. III. A wide bandwidth of 2.99 GHz (47.8%), 2 GHz (38.4%), and 5.17 GHz (55.9%) are obtained for Ant. I, Ant. II, and Ant. III, respectively. By employing the techniques of eliminating additional ground plane and using conformal ground at the cylindrical surface of the radially embedded probe feed DRA, the proposed antennas obtain a wider bandwidth with a compact size and maintain consistency in radiation patterns over the operating frequency bands. These features make them suitable for the use in UWB communication devices.

ACKNOWLEDGEMENT

The authors would like to thank Dassault Systèmes Simulia Corporation for providing a free version of CST Studio Suite Learning Edition.

REFERENCES

[1] Federal Communications Commission, "Revision of part 15 of the commission's rules regarding ultra-wideband transmission systems," *First Report and Order FCC 02-48*, 2002.

[2] Abedian, M., S. K. A. Rahim, S. Danesh, M. Khalily, and S. M. Noghabaei, "Ultrawideband dielectric resonator antenna with WLAN band rejection at 5.8 GHz," *IEEE Antennas and Wireless Propagation Letters*, Vol. 12, 1523–1526, 2013.

[3] Lee, J. C., "Ultra wideband internal antenna," US 7,042,414B1, May 2006.

[4] McCorkle, J. W., "Early results from the Army Research Laboratory ultrawide-bandwidth foliage penetration SAR," in *Underground and Obscured Object Imaging and Detection*, Vol. 1942, 88–95, Orlando, FL, United States, 1993.

[5] Ressler, M. A., "The army research laboratory ultra wideband BoomSAR," in *IGARSS '96. 1996 International Geoscience and Remote Sensing Symposium*, Vol. 3, 1886–1888, Lincoln, NE, USA, 1996.

[6] Ressler, M., L. Nguyen, F. Koenig, D. Wong, and G. Smith, "The Army Research Laboratory (ARL) synchronous impulse reconstruction (SIRE) forward-looking radar," in *Unmanned Systems Technology IX*, Vol. 6561, 35–46, Orlando, Florida, United States, 2007.

[7] Phelan, B. R., K. I. Ranney, K. A. Gallagher, J. T. Clark, K. D. Sherbondy, and R. M. Narayanan, "Design of ultrawideband stepped-frequency radar for imaging of obscured targets," *IEEE Sensors Journal*, Vol. 17, No. 14, 4435–4446, 2017.

[8] Chang, S., M. Wolf, and J. W. Burdick, "Human detection and tracking via ultra-wideband (UWB) radar," in *2010 IEEE International Conference on Robotics and Automation*, 452–457, Anchorage, AK, USA, 2010.

[9] Foo, S., "Ultrawideband monitoring systems and antennas," US Patent 008781563B2, Jul. 2014.
[10] Duan, Z. and J. Liang, "Non-contact detection of vital signs using a UWB radar sensor," *IEEE Access*, Vol. 7, 36 888–36 895, 2018.
[11] Apple, "Ultra wideband availability," https://support.apple.com/en-in/HT212274, 2023.
[12] Chen, Z. N., *Antennas for Portable Devices*, Wiley, 2007.
[13] Ryu, K. S. and A. A. Kishk, "UWB dielectric resonator antenna having consistent omnidirectional pattern and low cross-polarization characteristics," *IEEE Transactions on Antennas and Propagation*, Vol. 59, No. 4, 1403–1408, Apr. 2011.
[14] Chen, Z. N., X. H. Wu, H. F. Li, N. Yang, and M. Y. W. Chia, "Considerations for source pulses and antennas in UWB radio systems," *IEEE Transactions on Antennas and Propagation*, Vol. 52, No. 7, 1739–1748, Jul. 2004.
[15] Zhang, K., R. Tan, Z. H. Jiang, Y. Huang, L. Tang, and W. Hong, "A compact, ultrawideband dual-polarized vivaldi antenna with radar cross section reduction," *IEEE Antennas and Wireless Propagation Letters*, Vol. 21, No. 7, 1323–1327, 2022.
[16] Yang, H., X. Xi, Y. Zhao, L. Wang, and X. Shi, "Design of compact ultrawideband slot antenna with improved band-edge selectivity," *IEEE Antennas and Wireless Propagation Letters*, Vol. 17, No. 6, 946–950, Jun. 2018.
[17] Sang, L., J. Wang, Z. Liu, W. Wang, W. Huang, and H. Tu, "A UWB metal waveguide slot array antenna based on hybrid resonant structural components," *IEEE Antennas and Wireless Propagation Letters*, Vol. 22, No. 4, 923–927, Apr. 2023.
[18] Hayat, T., M. U. Afzal, F. Ahmed, S. Zhang, K. P. Esselle, and Y. Vardaxoglou, "Low-cost ultrawideband high-gain compact resonant cavity antenna," *IEEE Antennas and Wireless Propagation Letters*, Vol. 19, No. 7, 1271–1275, Jul. 2020.
[19] Liang, J., C. C. Chiau, X. Chen, and C. G. Parini, "Study of a printed circular disc monopole antenna for UWB systems," *IEEE Transactions on Antennas and Propagation*, Vol. 53, No. 11, 3500–3504, Nov. 2005.
[20] Majeed, A. H., A. S. Abdullah, K. Sayidmarie, R. A. Abd-Alhameed, F. Elmegri, and J. M. Noras, "Compact dielectric resonator antenna with band-notched characteristics for ultra-wideband applications," *Progress In Electromagnetics Research C*, Vol. 57, 137–148, 2015.
[21] Abedian, M., S. K. A. Rahim, S. Danesh, S. Hakimi, L. Y. Cheong, and M. H. Jamaluddin, "Novel design of compact UWB dielectric resonator antenna with dual-band-rejection characteristics for WiMAX/WLAN bands," *IEEE Antennas and Wireless Propagation Letters*, Vol. 14, 245–248, 2014.
[22] Balanis, C. A., *Antenna Theory: Analysis and Design*, John Wiley & Sons, 2016.
[23] Al-Azza, A. A., N. Malalla, F. Harackiewicz, and K. Han, "Stacked conical-cylindrical hybrid dielectric resonator antenna for improved ultrawide bandwidth," *Progress In Electromagnetics Research Letters*, Vol. 79, 79–86, 2018.
[24] Denidni, T. A., Z. Weng, and M. Niroo-Jazi, "Z-shaped dielectric resonator antenna for ultrawideband applications," *IEEE Transactions on Antennas and Propagation*, Vol. 58, No. 12, 4059–4062, Dec. 2010.
[25] Petosa, A., N. Simons, R. Siushansian, A. Ittipiboon, and M. Cuhaci, "Design and analysis of multisegment dielectric resonator antennas," *IEEE Transactions on Antennas and Propagation*, Vol. 48, No. 5, 738–742, May 2000.
[26] Trivedi, K. and D. A. Pujara, "Design and development of a wideband fractal tetrahedron dielectric resonator antenna with triangular slots," *Progress In Electromagnetics Research M*, Vol. 60, 47–55, 2017.
[27] Abedian, M., S. K. A. Rahim, and M. Khalily, "Two-segments compact dielectric resonator antenna for UWB application," *IEEE Antennas and Wireless Propagation Letters*, Vol. 11, 1533–1536, 2012.
[28] Trivedi, K. and D. Pujara, "Design and development of ultrawideband-stacked triangular prism-shaped dielectric resonator antenna," *Microwave and Optical Technology Letters*, Vol. 61, No. 5, 1193–1199, 2019.
[29] Chauhan, M., A. K. Pandey, and B. Mukherjee, "A novel compact cylindrical dielectric resonator antenna for wireless sensor network application," *IEEE Sensors Letters*, Vol. 2, No. 2, 1–4, Jun. 2018.
[30] Xia, Z.-X. and K. W. Leung, "3-D-printed wideband circularly polarized dielectric resonator antenna with two printing materials," *IEEE Transactions on Antennas and Propagation*, Vol. 70, No. 7, 5971–5976, Jul. 2022.
[31] Khalily, M., M. R. Kamarudin, M. Mokayef, and M. H. Jamaluddin, "Omnidirectional circularly polarized dielectric resonator antenna for 5.2-GHz WLAN applications," *IEEE Antennas and Wireless Propagation Letters*, Vol. 13, 443–446, 2014.
[32] Pan, Y.-M., K. W. Leung, and K. Lu, "Compact quasi-isotropic dielectric resonator antenna with small ground plane," *IEEE Transactions on Antennas and Propagation*, Vol. 62, No. 2, 577–585, Feb. 2014.
[33] Chen, T.-W., W.-W. Yang, Y.-H. Ke, and J.-X. Chen, "A circularly polarized hybrid dielectric resonator antenna with wide bandwidth and compact size," *IEEE Antennas and Wireless Propagation Letters*, Vol. 22, No. 3, 591–595, 2023.
[34] Fang, X. S., K. P. Shi, and Y. X. Sun, "Design of the single-/dual-port wideband differential dielectric resonator antenna using higher order mode," *IEEE Antennas and Wireless Propagation Letters*, Vol. 19, No. 9, 1605–1609, Sep. 2020.
[35] Mongia, R. K. and P. Bhartia, "Dielectric resonator antennas — A review and general design relations for resonant frequency and bandwidth," *International Journal of Microwave and Millimeter-Wave Computer-Aided Engineering*, Vol. 4, No. 3, 230–247, 1994.
[36] Thakur, A. and S. Bhattacharyya, "Radially embedded probe fed circular disc dielectric resonator antenna in S-band," in *International Conference on Devices, Sensors and Systems (CoDSS 2024)*, Tezpur, India, 2024.
[37] Ahmed, M. F., M. A. G. Mohamed, A. A. Shaalan, and W. S. El-Deeb, "A novel compact dual notch with high-gain multilayer dielectric resonator antenna for ultrawide-band applications," *Progress In Electromagnetics Research M*, Vol. 112, 127–137, 2022.
[38] Liu, N.-W., Y.-D. Liang, L. Zhu, Z.-X. Liu, and G. Fu, "A low-profile, wideband, filtering-response, omnidirectional dielectric resonator antenna without enlarged size and extra feeding circuit," *IEEE Antennas and Wireless Propagation Letters*, Vol. 20, No. 7, 1120–1124, Jul. 2021.
[39] Yamoun, J. B. and N. Aknin, "Wideband capability in embedded stacked rectangular dielectric resonator antenna for X-band applications," *Progress In Electromagnetics Research Letters*, Vol. 115, 19–25, 2024.
[40] Leonardi, O., M. G. Pavone, G. Sorbello, A. F. Morabito, and T. Isernia, "Compact single-layer circularly polarized antenna for short-range communication systems," *Microwave and Optical Technology Letters*, Vol. 56, No. 8, 1843–1846, Aug. 2014.